



**HAL**  
open science

## Photoactive materials prepared by homogeneous hydrolysis with thioacetamide: Part 2 – TiO/ZnO nanocomposites

Vendula Houšková, V. Václav Štengl, Snejana Bakardjieva, Nataliya Murafa

### ► To cite this version:

Vendula Houšková, V. Václav Štengl, Snejana Bakardjieva, Nataliya Murafa. Photoactive materials prepared by homogeneous hydrolysis with thioacetamide: Part 2 – TiO/ZnO nanocomposites. *Journal of Physics and Chemistry of Solids*, 2009, 69 (7), pp.1623. 10.1016/j.jpccs.2007.11.029 . hal-00522549

**HAL Id: hal-00522549**

**<https://hal.science/hal-00522549>**

Submitted on 1 Oct 2010

**HAL** is a multi-disciplinary open access archive for the deposit and dissemination of scientific research documents, whether they are published or not. The documents may come from teaching and research institutions in France or abroad, or from public or private research centers.

L'archive ouverte pluridisciplinaire **HAL**, est destinée au dépôt et à la diffusion de documents scientifiques de niveau recherche, publiés ou non, émanant des établissements d'enseignement et de recherche français ou étrangers, des laboratoires publics ou privés.

## Author's Accepted Manuscript

Photoactive materials prepared by homogeneous hydrolysis with thioacetamide: Part 2 – TiO<sub>2</sub>/ZnO nanocomposites

Vendula Houšková, Václav Štengl, Snejana Bakardjieva, Nataliya Murafa

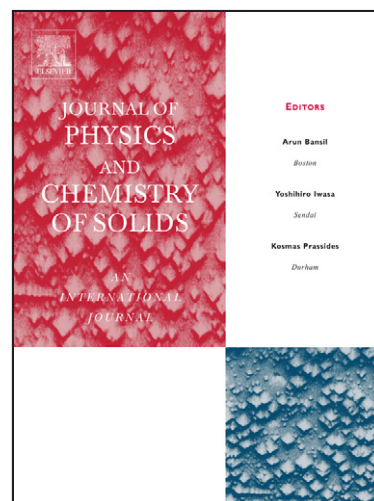
PII: S0022-3697(07)00754-8  
DOI: doi:10.1016/j.jpcs.2007.11.029  
Reference: PCS 5335

To appear in: *Journal of Physics and Chemistry of Solids*

Received date: 3 August 2007  
Revised date: 21 November 2007  
Accepted date: 30 November 2007

Cite this article as: Vendula Houšková, Václav Štengl, Snejana Bakardjieva and Nataliya Murafa, Photoactive materials prepared by homogeneous hydrolysis with thioacetamide: Part 2 – TiO<sub>2</sub>/ZnO nanocomposites, *Journal of Physics and Chemistry of Solids* (2007), doi:10.1016/j.jpcs.2007.11.029

This is a PDF file of an unedited manuscript that has been accepted for publication. As a service to our customers we are providing this early version of the manuscript. The manuscript will undergo copyediting, typesetting, and review of the resulting galley proof before it is published in its final citable form. Please note that during the production process errors may be discovered which could affect the content, and all legal disclaimers that apply to the journal pertain.



[www.elsevier.com/locate/jpcs](http://www.elsevier.com/locate/jpcs)

Photoactive materials prepared by homogeneous hydrolysis with  
thioacetamide:

Part 2 – TiO<sub>2</sub>/ZnO nanocomposites

Vendula Houšková\*<sup>1,2</sup>, Václav Štengl<sup>1</sup>, Snejana Bakardjieva<sup>1</sup>, Nataliya Murafa<sup>1</sup>,

<sup>1</sup>*Institute of Inorganic Chemistry, Academic of Sciences of the Czech Republic, Rez 250 68,*

*CZECH REPUBLIC*

<sup>2</sup>*University of Pardubice, Faculty of Chemical Technology, Institute of polymeric materials,*

*nám. Cs. Legií 562, Pardubice 532 10, CZECH REPUBLIC*

\*corresponding author: [houskova@iic.cas.cz](mailto:houskova@iic.cas.cz), tel.: 420 2 6617 3534, fax.: 420 2 2094 0257

**Abstract:** Photocatalytic active TiO<sub>2</sub>/ZnO composite was prepared by homogeneous hydrolysis of mixture of titanium oxo-sulphate and zinc sulphate in aqueous solutions with thioacetamide and subsequent annealing at temperature of 600 °C. The prepared samples were characterized by X-ray diffraction (XRD), Scanning electron microscopy (SEM), High resolution transmission microscopy (HRTEM). The nitrogen adsorption-desorption was used for surface area (BET) and porosity determination. The photoactivity of the prepared TiO<sub>2</sub>/ZnO samples was assessed by the photocatalytic decomposition of Orange II dye in aqueous slurry under irradiation of 254 nm and 365 nm wavelength. Under the same conditions, the photocatalytic activity of a commercially available photocatalyst (Degussa P25), the pure anatase TiO<sub>2</sub> nanoparticles and cubic ZnO were examined.

**Keywords:** A. zincite, A. anatase, A. rutile, B. homogeneous hydrolysis, D. photocatalytic activity

## 1. Introduction

Photocatalytic degradation processes have been widely applied as techniques of destruction of organic pollutants in wastewater and effluents. Titanium dioxide ( $\text{TiO}_2$ ) has been extensively investigated as one of the most active semiconductor photocatalysts [1]. It has been known that ZnO is a suitable alternative to  $\text{TiO}_2$  so far as band gap energy is concerned, and in fact higher photocatalytic efficiency compared with  $\text{TiO}_2$  has been reported for ZnO [2,3,4].

$\text{TiO}_2$  is widely used for photocatalytic air and water purification and many other purposes based on photocatalytic oxidation and decomposition of organic pollutants [5,6,7]. The material can be also used for solar energy storage and conversion [8], organic syntheses [9], etc. Titanium dioxide is one of the most popular and promising materials for these purposes, because of its stability, commercial availability and ecological safety. According to the literature [10,11,12], the photocatalytic activity of suspended  $\text{TiO}_2$  in solution strongly depends on the physical properties of  $\text{TiO}_2$  (e.g. crystallinity, crystal structure, surface area, surface hydroxyls and particle size).

In order to enhance the activity of catalyst, many efforts have been paid to modify  $\text{TiO}_2$  by adding ZnO as a photocatalyst [13,14,15]. Various preparation methods of ZnO nanoparticles [16,17,18,19,20] and their size dependent electronic [21] and optical [22] properties have been studied extensively for specific applications such as catalysts, photovoltaic and electroluminescent devices and functional devices (sensor, varistor, etc). In general, the physical, chemical and photochemical properties of the ZnO nanoparticles are different depending on the manufacturing method [23,24,25,26,27].

In this contribution, a binary oxide catalyst  $\text{TiO}_2/\text{ZnO}$  was prepared by a homogeneous hydrolysis of zinc sulfate, titanium oxo-sulphate ( $\text{TiOSO}_4$ ) and thioacetamide (TAA) at 80 °C and next control annealing in oxygen atmosphere at temperature of 600 °C. The photocatalytic activity of the  $\text{TiO}_2/\text{ZnO}$  composite was tested by degradation of an aqueous

solution of 0.02M Orange II dye at wavelengths of 254 and 365 nm. Under the same conditions, the photocatalytic activity of a commercially available photocatalyst (Degussa P25), the pure anatase  $\text{TiO}_2$  and ZnO [4] nanoparticles were examined.

## 2. Experimental

### 2.1. Synthesis of $\text{TiO}_2/\text{ZnO}$ nanocomposites

All used chemicals; titanium oxo-sulphate, zinc sulphate and thioacetamide (TAA) were of analytical grade and were supplied by Fluka.  $\text{TiOSO}_4$  and  $\text{ZnSO}_4 \cdot 7\text{H}_2\text{O}$  (see Table 1) was dissolved in 4 L of distilled water and 100g of thioacetamide was added. The reaction mixture was adjusted to the pH=2 with sulphuric acid. The reaction mixture was heated at temperature of 80 °C under stirring for 4 h. Thus-synthesized  $\text{TiO}_2/\text{ZnS}$  samples was washed with distilled water with decantation, filtered off, and dried at 105 °C in drying kiln. After atmosphere annealing at the temperature of 600 °C in oxygen atmosphere for 1 h, samples of  $\text{TiO}_2/\text{ZnO}$  nanocomposites were observed. By this method, twelve  $\text{TiO}_2/\text{ZnO}$  specimens denoted as TZO\_0 - TZO\_11 were prepared.

### 2.2. Characterization methods

Surface areas of the samples were determined from nitrogen adsorption-desorption isotherms at liquid nitrogen temperature using a Quantachrom Nova2000 instrument with outgas for 15 min at 150 °C. The Brunauer-Emmett-Teller (BET) method was used for surface area calculation [28]; the pore size distribution (pore diameter and pore volume of the samples) was determined by the Barrett-Joyner-Halenda (BJH) method [29].

Transmission electron microscopy (TEM and HRTEM) micrographs were obtained by using two instruments, namely, Philips EM 201 at 80 kV and JEOL JEM 3010 at 300 kV ( $\text{LaB}_6$  cathode). Copper grid coated with a holey carbon support film was used to prepare

samples for the TEM observation. A powdered sample was dispersed in ethanol and the suspension was treated in an ultrasonic bath for 10 minutes.

Scanning electron microscopy (SEM) studies were performed using a Philips XL30 CP microscope equipped with energy-dispersive X-ray (EDX), Robinson, secondary electron (SE) and back-scattered electron (BSE) detectors. The sample was placed on an adhesive C slice and coated with 10 nm thick layer of Au-Pd alloy.

X-ray diffraction (XRD) patterns were obtained by Siemens D5005 instrument using Cu K $\alpha$  radiation (40 kV, 30 mA) and diffracted beam monochromator. Qualitative analysis was performed with the Eva Application and the Xpert HighScore using the JCPDS PDF-2 database [30]. The crystallite sizes of the samples were calculated from the Scherrer equation [31] using the X-ray diffraction peak at  $2\Theta = 25.2^\circ$  (anatase), at  $2\Theta = 27.4^\circ$  (rutile), at  $2\Theta = 36.2^\circ$  (zincite) and at  $2\Theta = 35.1^\circ$  ( $\text{Zn}_2\text{TiO}_4$ ).

Photocatalytic activity of samples was assessed from the kinetics of the photocatalytic degradation of Orange II dye (OII) in aqueous slurries. Kinetics of the photocatalytic degradation of aqueous Orange II dye solution was measured by using a self-constructed photoreactor [32, 33]. The photoreactor consists of a stainless steel cover and quartz tube with florescent lamp (254 nm and 365 nm) with power 8W. Orange II dye solution circulated by means of a membrane pump through flow cuvette. The concentration of Orange II dye was determined by measuring the absorbance at 480 nm with VIS spectrofotometer ColorQuestXE.

### **3. Results and Discussion**

#### **3.1. X-Ray Diffraction (XRD)**

The powder XRD patterns of the  $\text{TiO}_2/\text{ZnO}$  composites prepared by homogeneous hydrolysis and subsequent annealing at  $600^\circ\text{C}$  are shown in Figure 1 and Figure 2. From the

XRD patterns and the corresponding characteristic  $2\Theta$  values of the diffraction peaks, it can be confirmed that the  $\text{TiO}_2$  in as-prepared samples was identified as anatase-phase (JC PDF 21-1272) or rutile-phase (JC PDF 21-1276), while the  $\text{ZnO}$  is zincite-phase (JC PDF 36-1451). In addition, zinc titanium oxide-phase (JC PDF 25-1164) was identified in some specimens. In samples TZO\_1 and TZO\_2, which were poorer in starting compound titanium oxo-sulphate, only two phases – zincite and zinc titanium oxide, occurred. Samples denoted as TZO\_3, TZO\_4 and TZO\_5 contain all four phases – anatase, rutile, zincite and zinc titanium oxide-phase. In case of samples TZO\_6, TZO\_7, TZO\_8, TZO\_9 and TZO\_10 lower content of zinc oxide forms with anatase some kind of intra-particle structure. Samples TZO\_0 and TZO\_11 are pure forms of anatase and zincite.

The average size  $t$  of crystallites was calculated from the peak half-width  $B$ , using the Sherrer equation [31],

$$t = \frac{k\lambda}{B \cos \Theta} \quad (1)$$

where  $k$  is a shape factor of the particle (it is 1 if the spherical shape is assumed) and  $\lambda$  and  $\Theta$  are the wavelength and the incident angle of the X-rays, respectively. The peak width was measured at half of the maximum intensity. The crystallite sizes were calculated from diffraction plane (101) of anatase, diffraction plane (111) of zincite, diffraction plane (110) of rutile and diffraction plane (100) of  $\text{Zn}_2\text{TiO}_4$ . The relative amount of anatase, rutile, zincite and  $\text{Zn}_2\text{TiO}_4$ , respectively, were calculated from XRD patterns by PowderCell for Windows version 2.1. programme (see Table 2).

### 3.2. Surface area and porosity

BET Langmuir surface area of  $\text{TiO}_2/\text{ZnO}$  composite depend on amount of  $\text{TiO}_2$ , the largest surface area ( $108.8 \text{ m}^2\text{g}^{-1}$ ) has sample denoted as TZO\_11 (see Table 1).  $\text{TiO}_2/\text{ZnO}$  nanocomposites displayed a type I isotherm with desorption hysteresis loop A [34]. Type a

hysteresis is due principally to cylindrical pores open at both ends and the microporosity of pore size distribution is most often about pore diameter of 0.17 nm. Results from desorption BJH pore volume distribution and pore area distribution confirmed microporous structure of prepared samples. Pore radius is in interval 0.15-0.25 nm and total pore volume is in interval 0.005-0.12 ccg<sup>-1</sup> for TiO<sub>2</sub>/ZnO nanocomposites.

### 3.3. Scanning electron microscopy (SEM)

The SEM micrographs of the prepared TiO<sub>2</sub>/ZnO nanocomposites are presented in Figure 3. It is obvious that annealed product of homogeneous precipitation of thioacetamide and zinc sulphate consists of approximate spherical round particle agglomerates of diameter about 2 μm (Figure 3e,f), which are formed by spherical nanoparticles conjoined to the chains [4]. The annealed product of homogeneous hydrolysis of thioacetamide and titanium oxo-sulphate consists of approximate spherical agglomerates of diameter about 1 μm (Figure 3k). The TiO<sub>2</sub>/ZnO composites are formed with mixture of single agglomerates of anatase, rutile, zincite or zinc titanium oxide. A special group is formed by overgrown agglomerates of TiO<sub>2</sub> and ZnO represented by TZO\_6 to TZO\_10 specimens.

### 3.4. High-resolution transmission electron microscopy (HRTEM)

Results obtained by high resolution transmission electron microscopy (HRTEM) are shown in Figure 4. The HRTEM micrographs in Figures 4a-d characterized the surface morphology of the sample denoted as TZO\_5. It is obvious that the nanoparticles of each phases form crystalline islands. The interlayer spacing is 0.352 nm, corresponding to the (101) plane of anatase (Figure 4d), the interlayer spacing 0.324 nm, corresponding to the (110) plane of rutile (Figure 4b, phase No. 4), the interlayer spacing 0.247 nm, corresponding



to the (101) plane of zincite (Figure 4c) and the interlayer spacing 0.596 nm, corresponding to the (100) plane of  $Zn_2TiO_4$  (Figure 4b, phase No. 3).

### 3.6. Photocatalytic activity

The photocatalytic activity of the prepared samples was determined by degradation of 0.02M Orange II dye aqueous solutions at 254 nm and 365nm radiation. In regions where is validated Lamber-Beer law, the concentration is proportional to absorbance.

$$A = \varepsilon c l \quad (3)$$

where  $A$  is absorbance,  $c$  is the concentration of the absorbing component,  $l$  is the length of the absorbing layer and  $\varepsilon$  is the molar absorbing coefficient. The time dependences of Orange II dye decomposition can be described by using Equation (4) for the first kinetics reaction[35]:

$$\frac{d[OII]}{dt} = k(a_0 - [OII]) \quad (4)$$

where  $[OII]$  is the concentration of Orange II dye,  $a_0$  is the initial concentration of Orange II dye, and  $k$  is the rate constant. For comparison, the photocatalytic activity of a commercially available photocatalyst Degussa P25, anatase  $TiO_2$  or  $ZnO$  nanoparticles were tested. The calculated degradation rate constants are listed in Table 3 and examples of kinetic degradation of Orange II dye at 254nm and 365nm wavelength using samples TZO\_0, TZO\_7, TZO\_10 and P25 are showed in Figure 5. The highest degradation rate was achieved over the sample TZO\_7 ( $k = 0.1232$ ). This result corresponds to the high BET surface area ( $61.7 \text{ m}^2\text{g}^{-1}$ ).

UV light provides the photons required for the electron transfer from valence band to conduction band of the photocatalyst. The energy of a photon is related to its wavelength and the overall energy input to a photocatalytic process is dependent upon the light intensity. Therefore, the effect of both intensity and wavelength is important. Matthews and McEvoy

[36] showed that shorter wavelength (254 nm) radiation is considerably more effective in promoting degradation than radiation centred at 350 nm and the optimum rate occurred with a lower catalyst loading than required at 350 nm. Hofstadler et al. [37] also showed that shorter wavelengths resulted in higher photocatalytic degradation process rates of 4-chlorophenol with small amounts of intermediates being formed. This is due to the fact that shorter wavelength is associated with greater photon energy.

#### 4. Conclusion

Nanocomposite of  $\text{TiO}_2/\text{ZnO}$  were prepared by homogeneous hydrolysis of zinc (II) sulphate and titanium oxo-sulphate in aqueous solution at temperature of 80 °C with thioacetamide and subsequent annealing at temperature of 600 °C. The solids consisted of uniform spherical aggregates in which the diameter of crystallites are decreasing with increasing amount of  $\text{TiO}_2$ .

It is obvious that BET surface areas (Table 1) are smaller in specimens doped with ZnO and annealed at higher temperatures. However, the photocatalytic activity of prepared samples was above-average. Specimens doped with ZnO showed higher photodegradation rate of Orange II and the highest degradation rate was achieved over sample denoted as TZO\_7 ( $k = 0,1232$ ) and all samples accomplished comparable photocatalytic properties to standard Degussa P25. Higher photocatalytic activity at 254 nm wavelength is given by higher band-gap energies of ZnO (3.3 eV) [38]. The higher photodegradation rate at 365 nm wavelength induces the smaller degradation rate at 254 nm wavelength.

#### Acknowledgements

This work was supported by the Academy of Sciences of the Czech Republic (Project No. AV OZ 40320502)

**References:**

1. A. Fujishima, T. N. Rao, D. A. Tryk, Titanium dioxide photocatalysis, *Journal of Photochemistry and Photobiology C: Photochemistry Reviews* 1 (2000), 1-21.
2. A.A. Khodja, T. Sehili, J.F. Pilichowski, P. Boule, Photocatalytic degradation of 2-phenylphenol on TiO<sub>2</sub> and ZnO in aqueous suspensions, *J. Photochem. Photobiol. A: Chem.* 141 (2001), 231–239.
3. C. Lizama, J. Freer, J. Baeza, H.D. Mansilla, Optimized photodegradation of Reactive Blue 19 on TiO<sub>2</sub> and ZnO suspensions, *Catal. Today* 76 (2002), 235–246.
4. V. Houšková, V. Štengl, S. Bakardjieva, N. Murafa, A. Kalendová, F. Opluštil, Nanostructure materials for destruction of warfare agents and eco-toxins prepared by homogeneous hydrolysis with thioacetamide: Part 1—zinc oxide, *Journal of Physics and Chemistry of Solids* 68 (2007), 716–720.
5. J.-M. Herrmann, J. Disdier, P. Pichat, S. Malato, J. Blanco, TiO<sub>2</sub>-based solar photocatalytic detoxification of water organic pollutants. Case studies of 2,4-dichlorophenoxyacetic acid (2,4-D) and of benzofuran, *Appl. Catal. B: Environ.* 17 (1998), 15–23.
6. P.V. Kamat, Photochemistry on nonreactive and reactive (semiconductor) surfaces, *Chem. Rev.* 93 (1993), 267–300.
7. M.R. Hoffmann, S.T. Martin, W. Choi, D.W. Bahnemann, Environmental Applications of Semiconductor Photocatalysis, *Chem. Rev.* 95 (1995), 69–96.
8. J. Bard, Design of Semiconductor Photoelectrochemical Systems for Solar Energy Conversion, *J. Phys. Chem.* 86 (1982), 172–177.
9. M.A. Fox, M.T. Dulay, Heterogeneous photocatalysis, *Chem. Rev.* 93 (1993), 341–357.
10. K. Kato, A. Tsuzuki, H. Taoda, Y. Torii, T. Kato, Y. Butsugan, Crystal structures of TiO<sub>2</sub> thin coatings prepared from the alkoxide solution via the dip-coating technique affecting the photocatalytic decomposition of aqueous acetic acid, *J. Mater. Sci.* 29 (1994), 5911 -5915.
11. R.R. Bacsa, J. Kiwi, Effect of rutile phase on the photocatalytic properties of nanocrystalline titania during the degradation of p-coumaric acid, *Appl. Catal. B Environ.* 16 (1998), 19-29.
12. V. Štengl, J. Šubrt, P. Bezdička, M. Maříková, S. Bakardjieva, Homogeneous precipitation with urea - An easy process for making spherical hydrous metal oxides, *Solid State Phen. V.* 90-91 (2003), 121-126.

13. H.-H. Ou, S.-L. Lo, Ch.-H. Wu, Exploring the interparticle electron transfer process in the photocatalytic oxidation of 4-chlorophenol *Journal of Hazardous Materials B* 137 (2006), 1362–1370.
14. G. Marci, V. Augugliaro, M. J. López-Munoz, C. Martín, L. Palmisano, V. Rives, M. Schiavello, R. J. D. Tilley, A. M. Venezia, Preparation Characterization and Photocatalytic Activity of Polycrystalline ZnO/TiO<sub>2</sub> Systems. 1. Surface and Bulk Characterization, *J. Phys. Chem. B* 105(5) (2001), 1026-1032.
15. S. Liao, H. Donggen, D. Yu, Y. Su, G. Juan, Preparation and characterization of ZnO/TiO<sub>2</sub>, SO<sub>4</sub><sup>2-</sup>/ZnO/TiO<sub>2</sub> photocatalyst and their photocatalysis, *Journal of Photochemistry and Photobiology A: Chemistry* 168 (2004), 7-13.
16. M.S. El-Shall, D. Graiver, U. Pernisz and M.I. Baraton, Synthesis and characterization of nanoscale zinc oxide particles: I. laser vaporization/condensation technique, *NanoStructured Mat.* 6 (1995), 297-300.
17. S. Hingorani, V. Pillai, P. Kumar, M.S. Multani and D.O. Shah, Microemulsion mediated synthesis of zinc-oxide nanoparticles for varistor studies, *Mat. Res. Bull.* 28 (1993), 1303-1310.
18. D. Kaneko, H. Shouji, T. Kawai and K. Kon-No, Synthesis of ZnO particles by ammonia-catalyzed hydrolysis of zinc dibutoxide in nonionic reversed micelles, *Langmuir* 16 (2000), 4086-4089.
19. T. Tani, L. Mädler and S.E. Pratsinis, Homogeneous ZnO nanoparticles by flame spray pyrolysis, *J. Nanoparticle Res.* 4 (2002), 337-343.
20. C. L. Carnes and K.J. Klabunde, Synthesis, Isolation, and Chemical Reactivity Studies of Nanocrystalline Zinc Oxide, *Langmuir* 16 (2000), 3764-3772.
21. M.F. Iskandar, K. Okuyama and F.G. Shi, Stable photoluminescence of zinc oxide quantum dots in silica nanoparticles matrix repared by the combined sol–gel and spray drying method, *J. Appl. Phys.* 89 (2001), 6431-6434.
22. M. Abdullah, S. Shibamoto and K. Okuyama, Synthesis of ZnO/SiO<sub>2</sub> nanocomposites emitting specific luminescence colors, *Opt. Mater.* 26 (2004), 95-100.

23. M.A. Valenzuela, P. Bosch, J. Jiménez-Becerrill, O. Quiroz, A.I. Páez, Preparation, characterization and photocatalytic activity of ZnO, Fe<sub>2</sub>O<sub>3</sub> and ZnFe<sub>2</sub>O<sub>4</sub>, *Journal of Photochemistry and Photobiology A: Chemistry* 148 (2002) 177–182.
24. L.Jing, Z.Xu, X.Sun, J.Shang, W.Cai, The surface properties and photocatalytic activities of ZnO ultrafine particles, *Applied Surface Science* 180 (2001), 308-314.
25. S.B.Park, Y.C.Kang, Photocatalytic Activity Of Nanometer Size ZnO Particles Prepared By Spray Pyrolysis, *J. Aerosol Sci.* 28 (1997), 473-474.
26. X. Ren, D. Han, D. Chen, F. Tang, Large-scale synthesis of hexagonal cone-shaped ZnO nanoparticles with a simple route and their application to photocatalytic degradation, *Materials Research Bulletin* 42 (2007), 807–813.
27. J. Nishio, M. Tokumura, H. T. Znad, Y. Kawase, Photocatalytic decolorization of azo-dye with zinc oxide powder in an external UV light irradiation slurry photoreactor, *Journal of Hazardous Materials B* 138 (2006), 106–115.
28. Brunauer S., P.H. Emmett, E. Teller, Adsorption of gases in multimolecular layers, *J. Am. Chem. Soc.* 60 (1938), 309-319.
29. Barret E.P., Joyner L.G., Halenda P.P., The Determination of Pore Volume and Area Distributions in Porous Substances. I. Computations from Nitrogen Isotherms, *Journal of The American Chemical Society* 73 (1951), 373-380.
30. JCPDS PDF-2 release 2001, ICDD Newtown Square, PA, USA.
31. A.L. Patterson, The Scherrer formula for X-ray particle size determination, *Phys. Rev.* 56 (1939), 978–982.
32. V. Štengl, S. Bakardjieva, N. Murafa, V. Balek, V. Havlín, Optically transparent titanium dioxide particles incorporated in hydroxyethyl methacrylate thin layers, *Advanced Synthesis & Catalysis*, in press.
33. J.M. Monteagudo, A. Durán, Fresnel lens to concentrate solar energy for the photocatalytic decoloration and mineralization of Orange 2 in aqueous solution, *Chemosphere* 65 (2006), 1242-1248.
34. S. Lowell, J.E. Shields, *Powder Surface Area and Porosity*, Chapman&Hall, London (1998).

35. M. Macounová, H. Krýsová, J. Ludvík, J. Jirkovský, Kinetics of photocatalytic degradation of diuron in aqueous colloidal solutions of Q-TiO<sub>2</sub> particles, *Journal of Photochemistry and Photobiology A: Chemistry* 156 (2003), 273-282.
36. R.W. Matthews, S.R. McEvoy, A comparison of 254 nm and 350 nm excitation of TiO<sub>2</sub> in simple photocatalytic reactors. *J. Photochem. Photobiol. A: Chem* 66 (1992), 355-366.
37. K. Hofstadler, R. Bauer, S. Novalic, G. Heisler, New reactor design for photocatalytic wastewater treatment with TiO<sub>2</sub> immobilized on fused silica glass fibers: photomineralization of 4-chlorophenol. *Environ. Sci. Technol.* 28 (1994), 670-674.
38. A. Mang, K. Reimann, S. Rübenacke, Band gaps, crystal-field splitting, spin-orbit coupling, and exciton binding energies in ZnO under hydrostatic pressure, *Solid State Communications* 94 (1995), 251-254.

**Figure Captions:**

Figure 1. XRD patterns of TiO<sub>2</sub>/ZnO composite (samples of TZO\_0 - TZO\_5).

Figure 2. XRD patterns of TiO<sub>2</sub>/ZnO composite (samples of TZO\_6 - TZO\_11).

Figure 3. SEM micrographs of particles prepared by homogenous hydrolysis and subsequent annealing at temperature of 600 °C for 1 h in oxygen atmosphere. a) TZO\_0, b) TZO\_1, c) TZO\_2, d) TZO\_3, e) TZO\_4, f) TZO\_5, g) TZO\_6, h) TZO\_7, i) TZO\_8, j) TZO\_9, l) TZO\_10, k) TZO\_11.

Figure 4. HRTEM micrographs of TZO\_5 sample. b) 1-zincite phase, 2-anatase phase, 3-zinc titanium oxide phase, 4-rutile phase; c) detail of zincite phase; d) detail of anatase phase.

Figure 5. Photodegradation of Orange II at wavelengths of 254 nm and 365 nm. Specimens of TiO<sub>2</sub>/ZnO composite (TZO\_1, TZO\_7 and TZO\_10) and the standard photocatalyst Degussa (P25).

**Tables:**

Table 1. Characteristics of prepared samples denoted as TZO\_0 to TZO\_11. Experimental conditions, Energy Dispersive X-ray analysis (EDX), BET surface areas and porosities of prepared samples.

Table 2. Crystallite sizes of the anatase, rutile, zincite and zinc titanium oxide phases contained in prepared TiO<sub>2</sub>/ZnO composites.

Table 3. Photodegradation rate of Orange II of prepared specimens and commercially available photocatalyst Degussa P25.

Accepted manuscript



Figure 1. – Houšková et al.

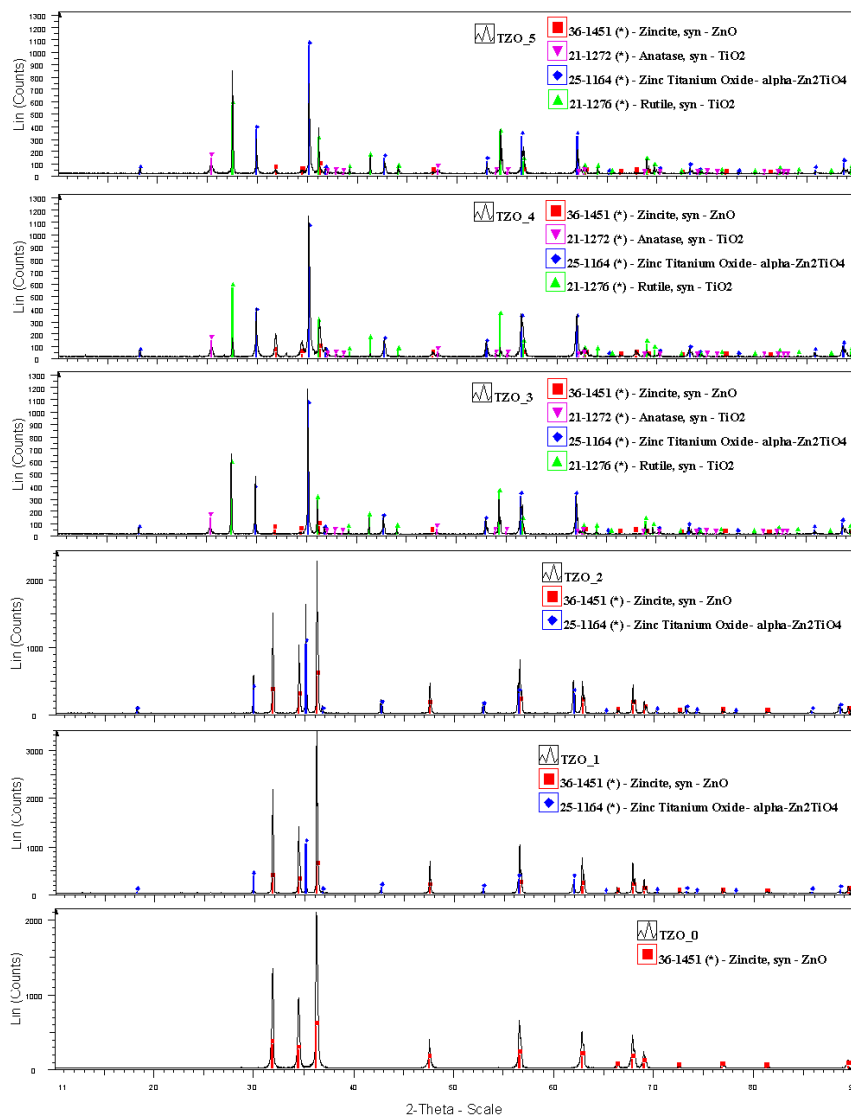


Figure 2. – Houšková et al.

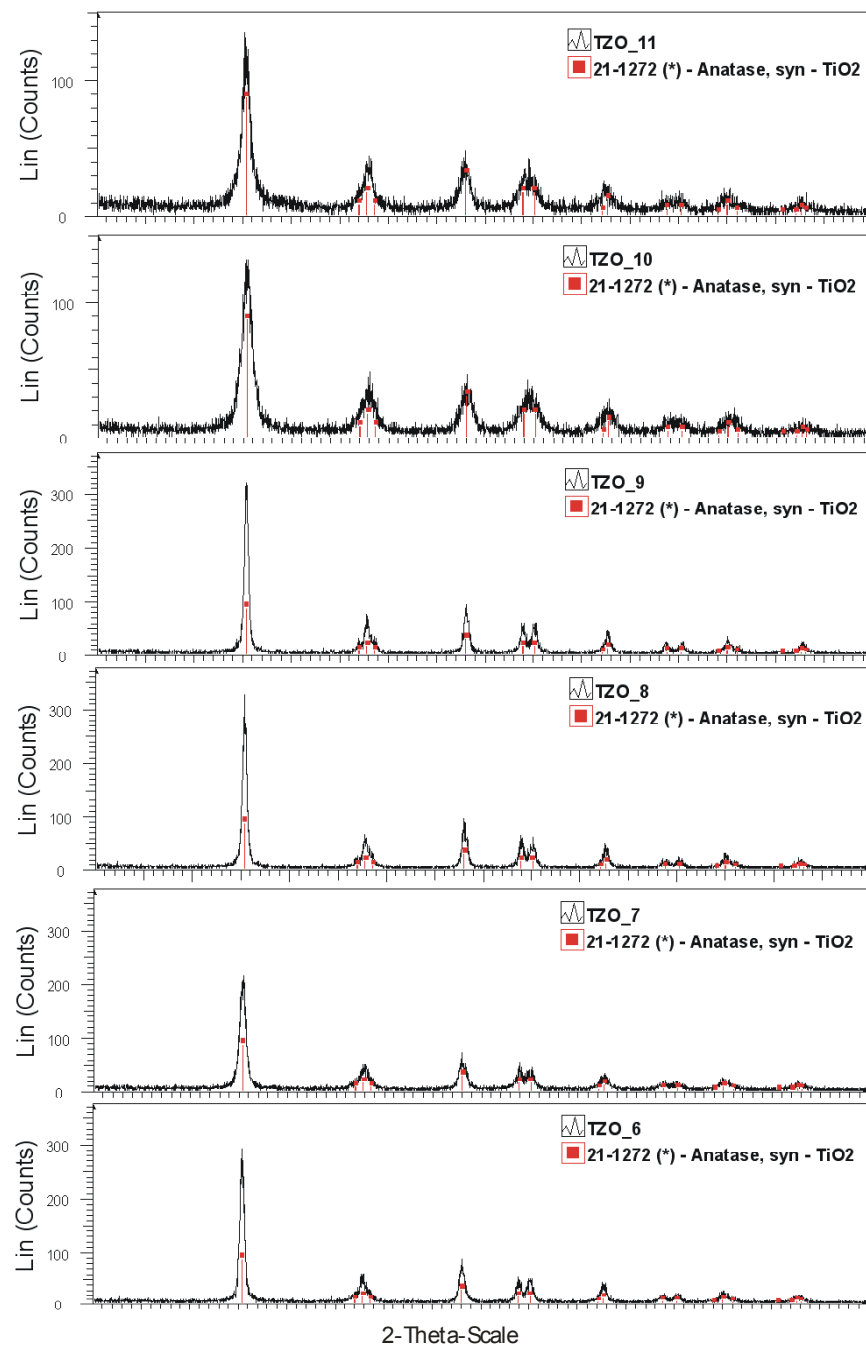


Figure 3. – Houšková et al.

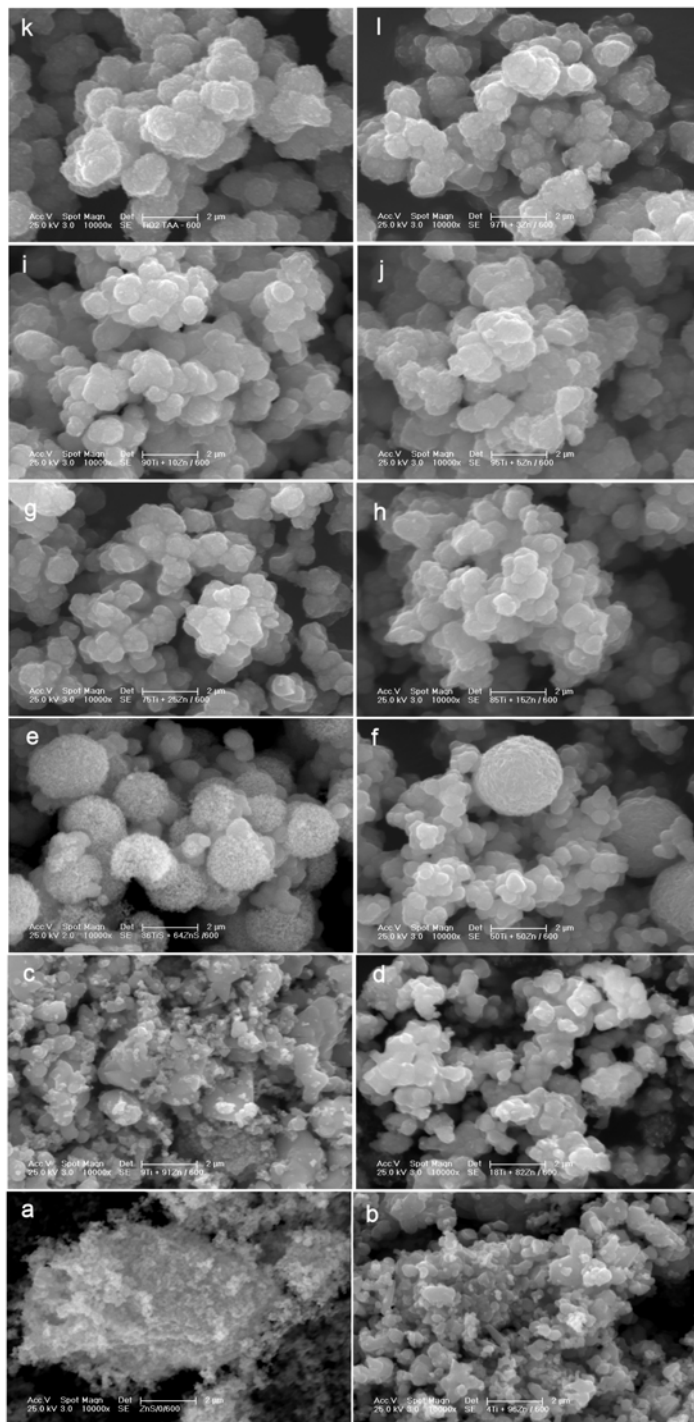


Figure 4. – Houšková et al.

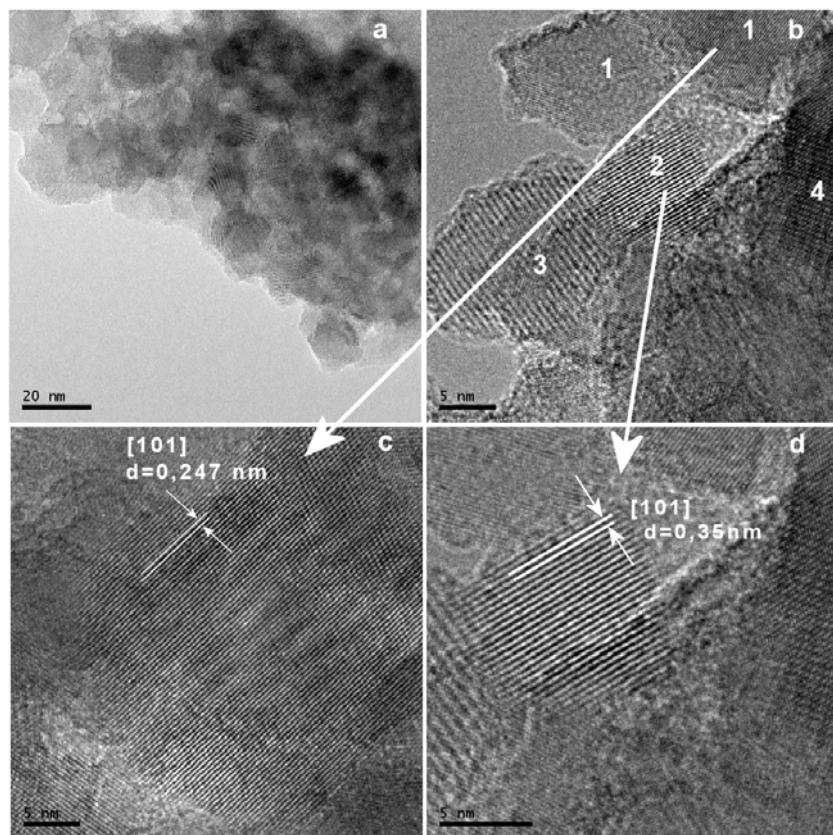


Figure 5. – Houšková et al.

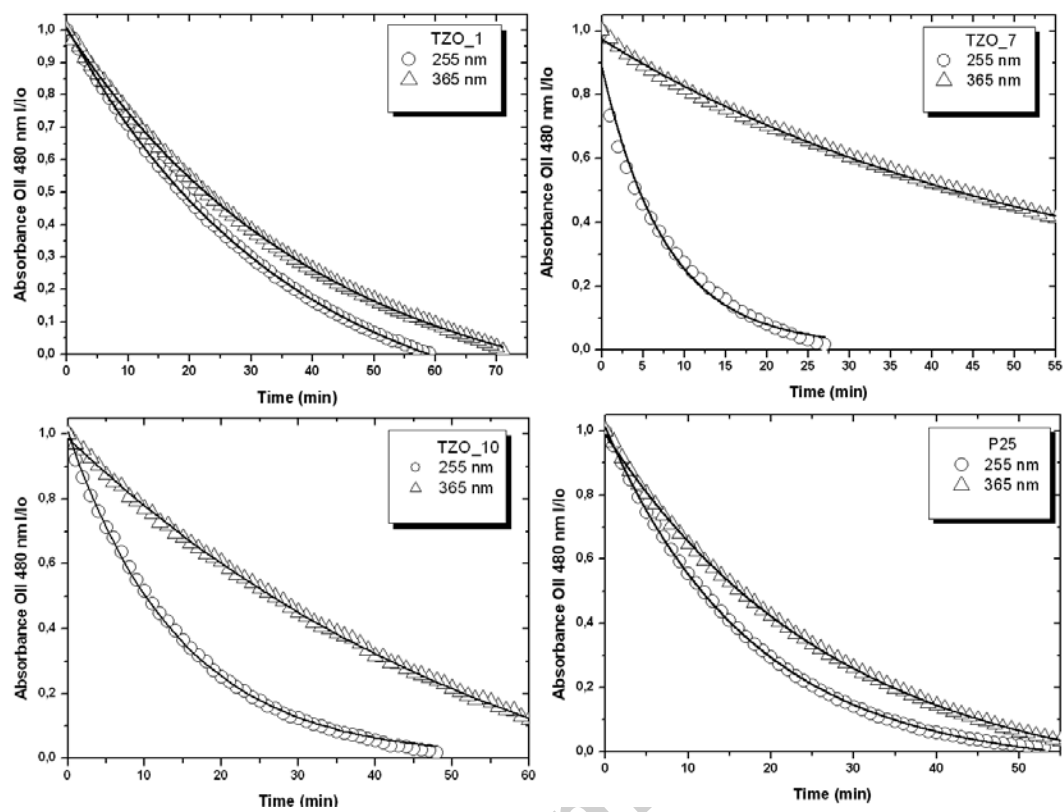


Table 1. – Houšková et al.

Sample	TiOSO <sub>4</sub> [g]	ZnSO <sub>4</sub> [g]	EDX of Ti [wt.%]	EDX of Zn [wt.%]	EDX of S [wt.%]	BET [m <sup>2</sup> g <sup>-1</sup> ]	Pore Radius [nm]	Pore Volume [ccg <sup>-1</sup> ]
TZO_0	0	100	-	82.09	0.86	5.6	0.17	0.018
TZO_1	4	96	3.53	78.92	0.11	6.9	0.17	0.011
TZO_2	9	91	7.70	70.25	0.21	12.5	0.15	0.018
TZO_3	18	82	30.71	30.85	0.76	2.9	0.17	0.005
TZO_4	36	64	32.18	26.45	0.65	10.4	0.17	0.018
TZO_5	50	50	34.25	21.19	0.82	28.2	0.17	0.041
TZO_6	75	25	44.43	1.44	0.71	37.4	0.17	0.041
TZO_7	85	15	54.97	1.55	1.11	61.7	0.17	0.065
TZO_8	90	10	54.35	0.26	0.77	66.9	0.19	0.093
TZO_9	95	5	50.12	0.12	0.54	72.5	0.24	0.105
TZO_10	97	3	48.90	0.5	0.71	79.6	0.25	0.115
TZO_11	100	0	56.23	-	0.30	108.8	0.17	0.121

Table 2. – Houšková et al.

Sample	Anatase crystallite size [nm]	Rutile crystallite size [nm]	Zincite crystallite size [nm]	Zn <sub>2</sub> TiO <sub>4</sub> crystallite size [nm]
TZO_0	-	-	63.2	-
TZO_1	-	-	85.6	63.6
TZO_2	-	-	82.5	82.2
TZO_3	21.6	115.9	79.3	60.1
TZO_4	22.2	120.4	78.2	59.6
TZO_5	22.8	122.7	78.6	53.9
TZO_6	15.2	-	-	-
TZO_7	2.6	-	-	-
TZO_8	3.0	-	-	-
TZO_9	5.2	-	-	-
TZO_10	6.2	-	-	-
TZO_11	6.2	-	-	-

Table 3. – Houšková et al.

Sample	Rate const. at 254 nm [min <sup>-1</sup> ]	Rate const. at 365 nm [min <sup>-1</sup> ]
TZO_0	0.0437	0.0211
TZO_1	0.0444	0.0355
TZO_2	0.0439	0.0194
TZO_3	0.0253	0.0114
TZO_4	0.0752	0.0209
TZO_5	0.0411	0.0086
TZO_6	0.0703	0.0092
TZO_7	0.1232	0.0155
TZO_8	0.0986	0.0121
TZO_9	0.0550	0.0120
TZO_10	0.0609	0.0233
TZO_11	0.0817	0.0340
P25 Degussa	0.0647	0.0471